

Multistate electron transfer dynamics in the condensed phase: Exact calculations from the reduced hierarchy equations of motion approach

Midori Tanaka^{a)} and Yoshitaka Tanimura^{b)}*Department of Chemistry, Graduate School of Science, Kyoto University, Kyoto 606-8502, Japan*

(Received 5 February 2010; accepted 20 April 2010; published online 1 June 2010)

Multiple displaced oscillators coupled to an Ohmic heat bath are used to describe electron transfer (ET) in a dissipative environment. By performing a canonical transformation, the model is reduced to a multilevel system coupled to a heat bath with the Brownian spectral distribution. A reduced hierarchy equations of motion approach is introduced for numerically rigorous simulation of the dynamics of the three-level system with various oscillator configurations, for different nonadiabatic coupling strengths and damping rates, and at different temperatures. The time evolution of the reduced density matrix elements illustrates the interplay of coherences between the electronic and vibrational states. The ET reaction rates, defined as a flux-flux correlation function, are calculated using the linear response of the system to an external perturbation as a function of activation energy. The results exhibit an asymmetric inverted parabolic profile in a small activation regime due to the presence of the intermediate state between the reactant and product states and a slowly decaying profile in a large activation energy regime, which arises from the quantum coherent transitions.

© 2010 American Institute of Physics. [doi:10.1063/1.3428674]

I. INTRODUCTION

The analysis of electron transfer (ET) processes is of great interest to a variety of researches in chemistry, biology, and physics.^{1–5} Most ET processes occur in condensed phases where the surrounding molecules provide the fluctuations and dissipation needed in the reactions.^{6–10} In a widely used model for ET problems, the electronic states are coupled to an intermediate harmonic nuclear or intramolecular vibrational mode, which is in turn coupled to a heat bath.^{11,12} This model describes fundamental chemical rate processes, interactions of a molecule with a dissipative and fluctuating environment,⁷ and Marcus theory for nonadiabatic ET.⁴ Further extensions of the model are used in laser spectroscopy to describe the coupling of electronic states to vibrational modes¹³ and the coupling of electronic states in solids to phonons.¹⁴ By adopting this description, one may study ET processes by nonlinear optical measurements with, for example, correlation function formalism based on the Liouville-space semiclassical propagation scheme,^{15–17} the diffusion-reaction equation method,¹⁸ the multistate quantum Fokker–Planck approach,^{19–21} or the multilevel Redfield theory.^{22–24} Tremendous insight was gained from this model from quantitative analytical calculations^{11,12,25–35} and numerical studies^{19–26,36–53} stimulated by experiments.^{18,54–61}

Many aspects have been discussed individually under some limited regime. In any approach, the full quantum treatment poses some difficult problems. While quantum nonadiabatic transitions in the absence of the bath can be studied by a wide variety of numerical methods based on the

wave function,⁶² a reduced density operator has to be used in the presence of the bath in order to study the irreversibility of system dynamics toward the thermal equilibrium state.⁶³

In the ET case, the harmonic mode of a nuclear or an intramolecular vibration can be included in the bath by carrying out a canonical transformation, which leads to a multilevel system coupled to the heat-bath with the canonically transformed spectral distribution function.¹¹ Then the reduction of the bath degrees of freedom can be performed using projection operator or path integral techniques.

While the projection operator approach and path integral approach are formally exact,^{64,65} one has to employ some approximation to derive reduced equation of motion such as the multilevel Redfield equation,^{22–24,36} the mixed quantum-classical equations of motion^{25,26} and stochastic Liouville equations,^{37,38,41–44} which can be solved numerically. The master equation approach requires several crucial assumptions, such as the rotating wave approximation, the white noise (or Van Hove) approximation, and the factorized initial condition. These approximations strongly limit the equation's applicability especially at a low temperature, where quantum effects play a major role.

The path integral approach, where the reduced density matrix elements are expressed in terms of the nonadiabatic interactions in functional form, is powerful for a strong system-bath coupling.^{11,12,27,28} However, since this approach handles nonadiabatic coupling perturbatively, it is not easy to study strong nonadiabatic (diabatic) coupling. Path integral Monte Carlo simulations can remove this limitation, but their applicability is limited because of the sampling processes.^{39,40} Note that the linear and nonlinear optical response functions obtained from cumulant expansion ap-

^{a)}Electronic mail: midori@kuchem.kyoto-u.ac.jp.^{b)}Electronic mail: tanimura@kuchem.kyoto-u.ac.jp.

proaches have a similar form as the perturbative results from path integrals since laser interactions play a similar role as the nonadiabatic coupling.^{15–17}

To eliminate all of the above mentioned limitations, one can derive the hierarchy equations of motion for the reduced density matrix by differentiating the reduced density matrix elements defined by path integrals.⁶³ This approach was first introduced to investigate the connection between the phenomenological stochastic Liouville equation theory and the dynamical Hamiltonian theory and was limited to the case in which the spectral distribution function is given by the Drude form (Ohmic form with a Lorentzian cutoff) and the bath temperature is relatively high.⁶⁶ By including low temperature correction terms, the temperature limitation can be eliminated.^{63,67–71} This formalism is valuable since it can handle not only the strong system-bath coupling but also quantum coherence between the system and bath which plays an important role for the electronic energy transfer in photosynthetic antenna system.^{72,73}

Although the form of hierarchy becomes complicated, it is possible to derive the hierarchy equations of motion for non-Ohmic spectral distributions.⁶⁷ If one applies the hierarchy formalism to the Brownian spectral distribution that arises from the canonical transformation of ET system, one can handle the ET problem in a nonperturbative manner for both the system-bath and nonadiabatic couplings.¹⁹ While the previously derived hierarchy equations for a two-state ET system cannot be applied to a low-temperature system, where the quantum transition plays a major role, we can remove this limitation by introducing the low temperature correction terms for the Brownian spectral distribution hierarchy.⁷⁴ Moreover, we can formulate the equations of motion for a multistate system, where the interplay between the sequential and superexchange ET transitions becomes important.^{29–35,39}

A typical example of three-state problem is bacterial photosynthesis where the ET takes place between the excited special pair to the bacteriopheophytin mediated by the accessory chlorophyll II monomer stationed in between them.⁷⁵ Many experimental and theoretical studies have been carried out to explore the mechanism of the primary ET step in photosynthetic bacteria.^{31–33,40,55–58}

In this paper, we present a complete study of the various nonperturbative regimes of ET processes, using the hierarchy of quantum kinetic equations. The present numerical study allows us to demonstrate a number of features arising from the interplay between quantum nonadiabatic transitions and dissipation. The organization of this paper is as follows. The model Hamiltonian and the hierarchy equations of motion for the canonically transformed Hamiltonian with the Brownian spectral distribution, including the low temperature correction terms, are presented in Sec. II. The time evolution of a three-state system is studied by numerically solving the hierarchy equations over wide parameter ranges in Sec. III. The ET rates as a function of temperature and activation energy are presented and discussed in Sec. IV. The last section is devoted to concluding remarks.

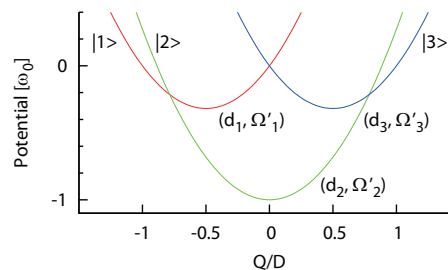


FIG. 1. Schematic view of a three-state system coupled to a harmonic mode. The parabolic potential for the state $|j\rangle$ has the vertex (d_j, Ω'_j) , where $\Omega'_j = \Omega_j - \lambda d_j^2$. The red, green, and blue lines are for the $|1\rangle$, $|2\rangle$, and $|3\rangle$ states, respectively. Here, parameters are the same as at the beginning of III.

II. HIERARCHY EQUATIONS OF MOTION FOR THE REDUCED DENSITY MATRIX ELEMENTS

We consider the case that the electronic energy states are coupled to an intermediate harmonic nuclear or intramolecular vibrational mode with P , Q , M , and ω_0 being its momentum, coordinate, mass, and frequency (see Fig. 1). To distinguish it from the bath modes, hereafter we refer to this mode as the (P, Q) oscillator mode. In this paper, we limit our analysis to the three-state case since the extensions to four or more states are straightforward. The oscillator states further couple to the bath represented by an ensemble of harmonic oscillators. This leads to a commonly used model for ET problems, which is expressed as^{11,12}

$$\hat{H} = \hat{H}_A - \sum_{j=1}^3 M \omega_0^2 Q d_j D |j\rangle \langle j| + \frac{P^2}{2M} + \frac{1}{2} M \omega_0^2 Q^2 + \sum_{\alpha} \left\{ \frac{p_{\alpha}^2}{2m_{\alpha}} + \frac{1}{2} m_{\alpha} \omega_{\alpha}^2 \left(x_{\alpha} - \frac{c_{\alpha}}{m_{\alpha} \omega_{\alpha}^2} Q \right)^2 \right\}, \quad (1)$$

where the system Hamiltonian is defined by

$$\hat{H}_A = \sum_{j=1}^3 \hbar \Omega_j |j\rangle \langle j| + \sum_{j=1, k \neq j}^3 \hbar \Delta_{jk} |j\rangle \langle k|. \quad (2)$$

Here, $\hbar \Omega_j$ is the energy of the electronic state $|j\rangle$, $\hbar \Delta_{j,k}$ is the transfer coupling between the j th and k th states, and $d_j D$ represents the displacement of the (P, Q) mode for $|j\rangle$, where D is the characteristic length of the system. The coordinate, momentum, mass, and frequency of the bath mode α is denoted by x_{α} , p_{α} , m_{α} , and ω_{α} . The constant c_{α} is the coupling strength to the mode α . The character of the bath is determined by the spectral distribution function $J(\omega) = \sum_{\alpha} c_{\alpha}^2 \delta(\omega - \omega_{\alpha}) / (2m_{\alpha} \omega_{\alpha})$. Here we consider the Ohmic case that is defined by $J(\omega) = M \gamma \omega$.

If the potential surface of the (P, Q) mode are anharmonic, one has to explicitly deal with the (P, Q) degrees of freedom by employing the multistate descriptions of the quantum kinetic equation^{20,21} or semiclassical kinetic equation.^{25,26,38} However, if the (P, Q) potential is harmonic, we can reduce the (P, Q) degrees of freedom into the bath, which allows us to simplify the ET problem and save the central processing unit power dramatically. This simplification is necessary to handle the multidimensional hierarchy arising from the low-temperature correction terms.^{63,67,68,70,71}

By performing the canonical transformation,¹¹ the Hamiltonian of this model is converted to that of the three-state system directly coupled to a bath of infinitely many harmonic oscillators with a significantly different bath spectral density

$$\hat{H} = \hat{H}_A - \hat{V} \sum_{\alpha} c'_{\alpha} x'_{\alpha} + \sum_{\alpha} \left(\frac{p'_{\alpha}{}^2}{2m'_{\alpha}} + \frac{1}{2} m'_{\alpha} \omega'_{\alpha}{}^2 x'_{\alpha}{}^2 \right), \quad (3)$$

where the system-bath coupling \hat{V} is written as

$$\hat{V} = \sum_{j=1}^3 d_j |j\rangle \langle j|, \quad (4)$$

and x'_{α} , p'_{α} , m'_{α} , ω'_{α} , and c'_{α} are the transformed α th coordinate, momentum, mass, frequency, and coupling strength, respectively. The spectral distribution function $J'(\omega) = \sum_{\alpha} c'_{\alpha}{}^2 \delta(\omega - \omega'_{\alpha}) / (2m'_{\alpha} \omega'_{\alpha})$ is also transformed as¹¹

$$J'(\omega) = \frac{2\hbar\lambda}{\pi} \cdot \frac{\gamma\omega_0^2\omega}{(\omega_0^2 - \omega^2)^2 + \gamma^2\omega^2}, \quad (5)$$

where $\lambda = MD^2\omega_0^2/2\hbar$. We refer to the above spectral distribution as the Brownian form since it arises from the correlation function of the Brownian oscillator system.^{27,28} The distribution is characterized by the characteristic frequency ω_0 , the displacement λ , and the coupling strength between the (P, Q) oscillator and the bath γ . The peak position and the peak width of $J'(\omega)$ change with γ .

The reduced density matrix element is expressed in the path integral form as (see Appendix A)

$$\rho(\bar{\psi}, \psi'; t) = \int D[\psi(\tau)] D[\bar{\psi}(\tau)] D[\psi'(\tau)] D[\bar{\psi}'(\tau)] \times e^{iS_A[\bar{\psi}, \psi, \bar{\psi}', \psi'; t]} F[\bar{\psi}, \psi, \bar{\psi}', \psi'; t] e^{-iS_A[\bar{\psi}', \psi', t]}, \quad (6)$$

where $\int D[\psi(\tau)]$ represents the functional integral of a set of Grassmann variables $\psi = \{\phi_1, \phi_2\}$ which describe the three system states. The action for the system's Hamiltonian is denoted by $S_A[\bar{\psi}, \psi]$. The bath effects are described by the Feynman-Vernon influence functional $F[\bar{\psi}, \psi, \bar{\psi}', \psi'; t]$.⁶⁴ For the distribution Eq. (5), the influence functional is calculated as⁷⁴

$$F[\bar{\psi}, \psi, \bar{\psi}', \psi'; t] = \exp \left[- \int_{t_0}^t ds \int_{t_0}^s du V^{\times}(s) (\Theta_{-}(u) e^{-(\gamma/2 - i\xi)(s-u)} + \Theta_{+}(u) e^{-(\gamma/2 + i\xi)(s-u)}) \right] \times \exp \left[\int_{t_0}^t ds \int_{t_0}^s du V^{\times}(s) \sum_{k=1}^{\infty} \Psi_k(u) \nu_k e^{-\nu_k(s-u)} \right], \quad (7)$$

where

$$\Theta_{\pm}(u) = \frac{\lambda\omega_0^2}{2\xi} \left\{ \pm \coth \left(\mp \frac{\beta\hbar\xi}{2} + i \frac{\beta\hbar\gamma}{4} \right) V^{\times}(u) \mp V^{\circ}(u) \right\}, \quad (8)$$

and

$$\Psi_k(u) = \frac{4\lambda}{\beta\hbar} \frac{\gamma\omega_0^2}{(\omega_0^2 + \nu_k^2)^2 - \gamma^2\nu_k^2} V^{\times}(u), \quad (9)$$

with $\xi = \sqrt{\omega_0^2 - \gamma^2/4}$ for $\gamma < 2\omega_0$ and $\nu_k = (2\pi/\beta\hbar)k$ with $2\pi/\beta\hbar$ being the Matsubara frequency. We denote $V^{\times}(t) \equiv V(\bar{\psi}(t), \psi(t)) - V(\bar{\psi}'(t), \psi'(t))$ and $V^{\circ}(t) \equiv V(\bar{\psi}(t), \psi(t)) + V(\bar{\psi}'(t), \psi'(t))$.

If we choose K so as to satisfy

$$\nu_K = \frac{2\pi}{\beta\hbar} K \gg \max\{\Omega_l - \Omega_m\}_{l,m}, \quad (10)$$

the function $e^{-\nu_k(s-u)}$ for $k \geq K$ in Eq. (7) can be replaced by the Dirac's delta function $\nu_k e^{\nu_k(s-u)} \approx \delta(s-u)$. This leads the influence functional Eq. (7) to

$$F[\bar{\psi}, \psi, \bar{\psi}', \psi'; t] = \exp \left[- \int_{t_0}^t ds \int_{t_0}^s du V^{\times}(s) (\Theta_{-}(u) e^{-(\gamma/2 - i\xi)(s-u)} + \Theta_{+}(u) e^{-(\gamma/2 + i\xi)(s-u)}) \right] \times \exp \left[\int_{t_0}^t ds \int_{t_0}^s du V^{\times}(s) \sum_{k=1}^K \Psi_k(u) \nu_k e^{-\nu_k(s-u)} \right] \times \exp \left[\int_{t_0}^t ds \Xi(s) \right], \quad (11)$$

where

$$\Xi(s) = V^{\times}(s) \sum_{k=K+1}^{\infty} \Psi_k(s). \quad (12)$$

The equation of motion for the reduced density operator can be derived by evaluating the time derivative of the left- and right-hand-side wave functions and the influence functional.^{63,66,70,71} If we consider the auxiliary matrix defined by

$$\rho_{j_1, j_2, \dots, j_K}^{(n,m)}(\bar{\psi}, \psi'; t) = \int D[\bar{\psi}(\tau)] D[\psi(\tau)] D[\bar{\psi}'(\tau)] D[\psi'(\tau)] \times e^{iS_A[\bar{\psi}, \psi, \bar{\psi}', \psi'; t]} F_{j_1, \dots, j_K}^{(n,m)}[\bar{\psi}, \psi, \bar{\psi}', \psi'; t] e^{-iS_A[\bar{\psi}', \psi', t]}, \quad (13)$$

where

$$\begin{aligned}
F_{j_1, \dots, j_K}^{(n,m)}[\bar{\psi}, \psi, \bar{\psi}', \psi'; t] = & \left\{ \int_{t_0}^t du \Theta_{-}(u) e^{-(\gamma/2 - i\zeta)(t-u)} \right\}^n \\
& \times \left\{ \int_{t_0}^t du \Theta_{+}(u) e^{-(\gamma/2 + i\zeta)(t-u)} \right\}^m \\
& \times \prod_{k=1}^K \left\{ \int_{t_0}^t du \Psi_k(u) e^{-\nu_k(t-u)} \right\}^{j_k} \\
& \times F[\bar{\psi}, \psi, \bar{\psi}', \psi'; t], \quad (14)
\end{aligned}$$

the equation of motion is derived in the hierarchy form as⁷⁴

$$\begin{aligned}
\frac{d}{dt} \hat{\rho}_{j_1, \dots, j_K}^{(n,m)}(t) = & -\hat{\mathcal{L}}^{(n,m)} \hat{\rho}_{j_1, \dots, j_K}^{(n,m)}(t) \\
& + \hat{V}^{\times} \hat{\rho}_{j_1, \dots, j_K}^{(n+1,m)}(t) + n \hat{\Theta}_{-} \hat{\rho}_{j_1, \dots, j_K}^{(n-1,m)}(t) \\
& + \hat{V}^{\times} \hat{\rho}_{j_1, \dots, j_K}^{(n,m+1)}(t) + m \hat{\Theta}_{+} \hat{\rho}_{j_1, \dots, j_K}^{(n,m-1)}(t) \\
& + \sum_{k=1}^K \hat{V}^{\times} \hat{\rho}_{j_1, \dots, j_{k+1}, \dots, j_K}^{(n,m)}(t) \\
& + \sum_{k=1}^K j_k \nu_k \hat{\Psi}_k \hat{\rho}_{j_1, \dots, j_{k-1}, \dots, j_K}^{(n,m)}(t), \quad (15)
\end{aligned}$$

where

$$\hat{\mathcal{L}}^{(n,m)} = \frac{i}{\hbar} \hat{H}_A^{\times} + \frac{(n+m)\gamma}{2} - i(n-m)\zeta + \sum_{k=1}^K j_k \nu_k - \hat{\Xi} \quad (16)$$

and $\hat{\Theta}_{\pm}$, $\hat{\Psi}_k$, and $\hat{\Xi}$ are the operator forms of Eqs. (8), (9), and (12) which are obtained by replacing $V^{\times} \rho$ with $\hat{V} \hat{\rho} - \hat{\rho} \hat{V}$ and $V^{\circ} \rho$ with $\hat{V} \hat{\rho} + \hat{\rho} \hat{V}$.

As can be seen from the form of equations, the (n, m, j_1, \dots, j_K) th member of the hierarchy is coupled to the lower- and higher-order members as $\hat{\rho}_{j_1, \dots, j_K}^{(n\pm 1, m)}$, $\hat{\rho}_{j_1, \dots, j_K}^{(n, m\pm 1)}$, $\hat{\rho}_{j_1 \pm 1, \dots, j_K}^{(n, m)}$, etc. In this approach, the zeroth member of the hierarchy is the exact solution of the total Hamiltonian Eq. (3) defined by $\hat{\rho}_{0, \dots, 0}^{(0,0)}(t) = \text{tr}_{x'} \{ \hat{\rho}_{\text{tot}}(t) \}$ and it includes all orders of the system-bath interactions. Then the orders of system-bath interactions in $\hat{\rho}_{j_1, \dots, j_K}^{(n, m)}$ are lower than that in $\hat{\rho}_{0, \dots, 0}^{(0,0)}$ by $N(N \equiv n+m + \sum_k j_k)$, since we defined the time derivative of F in Eq. (14) by excluding the factor $(V^{\times})^N$. Thus, the present approach conceptually differs from the conventional perturbative expansion approaches; in such approaches, the zeroth member includes no system-bath interactions and thus higher members take into account higher-order system-bath interactions.⁶³ Because of this hierarchical structure, we can handle strong system-bath interactions and non-white-noise baths.

For the condition

$$n + m + \sum_{k=1}^K j_k = N_{\text{max}} \gg \frac{\max\{\Omega_l - \Omega_m\}_{l,m}}{\min\left(\frac{\gamma}{2}, \nu_1\right)}, \quad (17)$$

this infinite hierarchy can be truncated by the terminator as

$$\frac{d}{dt} \hat{\rho}_{j_1, \dots, j_K}^{(n,m)}(t) = - \left[\frac{i}{\hbar} \hat{H}_A^{\times} - i(n-m)\zeta - \hat{\Xi} \right] \hat{\rho}_{j_1, \dots, j_K}^{(n,m)}(t). \quad (18)$$

The derivation of Eqs. (15) and (18) are given in Appendix A.

III. TIME-EVOLUTION OF DENSITY MATRIX ELEMENTS

We fix the frequency of the oscillators in the (P, Q) space as $\omega_0 = 500 \text{ cm}^{-1}$ ($1/\omega_0 = 66.7 \text{ fs}$) and use it as the unit of the system. The vibrational motion along the reaction coordinate is in the quantum regime at room temperature, since we have $\beta \hbar \omega_0 = 2.40$ for $T = 300 \text{ K}$.

Throughout this paper, we also fix the energies of $|3\rangle$ as $\Omega_3 = 0$, the nonadiabatic coupling between $|1\rangle$ and $|3\rangle$ as $\Delta_{13} = \Delta_{31} = 0$ and the individual coupling constants between the electronic state and the oscillator mode as $d_1 = -0.5$, $d_2 = 0$, and $d_3 = 0.5$. The displacement of the (P, Q) oscillators λ , the coupling strength between the oscillators and the bath γ , the temperature T , the energy of the initial and the intermediate state Ω_1 and Ω_2 are then changed independently to study the parameter dependence on $\hat{\rho}(t)$ and the ET reaction rate. In Secs. III and IV we set $\Omega_2 = -\omega_0$, $\Delta_{12} = \Delta_{21} = 0.1\omega_0$, and $\Delta_{23} = \Delta_{32} = 0.1\omega_0$ unless otherwise noted.

To calculate the time evolution of the density matrix elements, we set the initial populations as $\rho_1(0) = 1$ and $\rho_2(0) = \rho_3(0) = 0$, where $\rho_j(t)$ represents the population of the $|j\rangle$ state at time t . Experimentally such an initial condition can be prepared by applying a short laser pulse to instantaneously excite the $|1\rangle$ state.

The hierarchy equations of motion for the reduced density matrix Eqs. (15) and (18) are then solved via the fourth-order Runge–Kutta method, in which the time step is $0.01/\omega_0$. We chose the depth of the hierarchy and the truncation number of the hierarchy $K=5$ and $N=15$ for a low temperature case ($T=10 \text{ K}$), $K=3$ and $N=15$ for intermediate temperature cases ($120 \text{ K} \leq T \leq 600 \text{ K}$), $K=2$ and $N=15$ for $T=900 \text{ K}$, and $K=1$ and $N=15$ for high temperature cases ($T \geq 1500 \text{ K}$), respectively. For all calculations, the accuracies were checked by changing the values of K and N .

A. Effects of the displacement λ

Figures 2(a)–2(e) show the time evolution of the density matrix elements for various displacements of the (P, Q) oscillators represented by λ . Here, we chose $\gamma = 0.1\omega_0$ and $T = 300 \text{ K}$. Figure 2(a) illustrates the case that the displacements between the oscillators are zero ($\lambda = 0$). In this case, the profiles of wavepackets in each (P, Q) potentials in the $|1\rangle$, $|2\rangle$, and $|3\rangle$ states do not change via the nonadiabatic transitions due to their optical Condon transitionlike character.^{27,28} Since the heat bath can affect the system only through the (P, Q) space wavepacket dynamics and the wavepackets are already in the equilibrium profiles with the temperature T , the heat bath does not play any role if the displacement D is zero. Thus, the time evolution of $\rho_j(t)$, which reflects not the profile but the population of the j th wavepackets, exhibits only coherent motions between the three states. The frequencies of coherent motion can be ana-

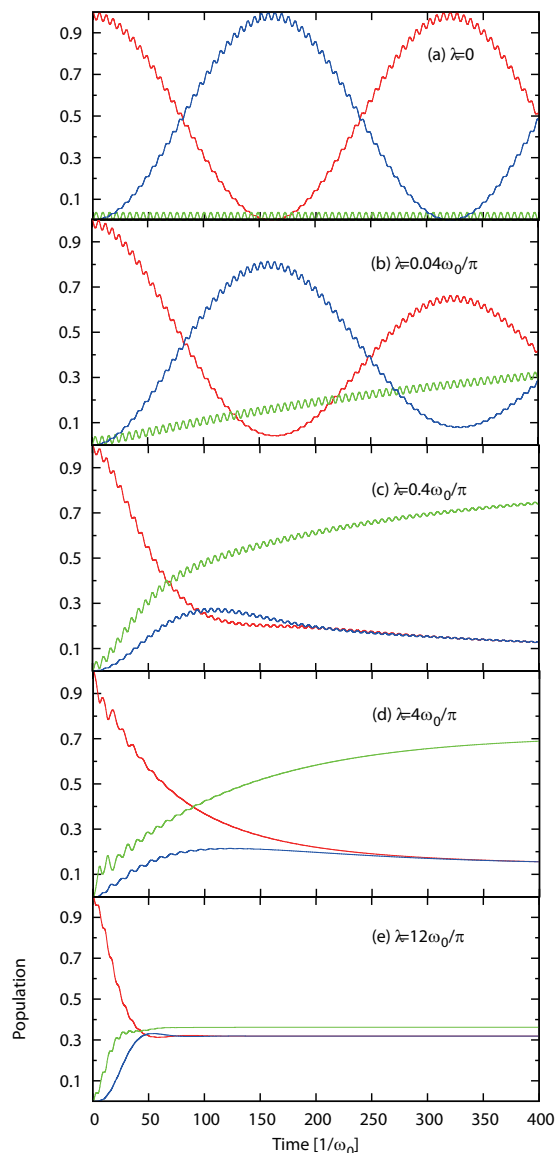


FIG. 2. Time-evolution of the density matrix elements for the different displacement of (P, Q) oscillators $\lambda =$ (a) 0, (b) $0.04\omega_0/\pi$, (c) $0.4\omega_0/\pi$, (d) $4\omega_0/\pi$, and (e) $12\omega_0/\pi$. We chose $\gamma = 0.1\omega_0$, $\Omega_2 = -\omega_0$, and $T = 300$ K. In each figure, the red, green, and blue lines show $\rho_1(t)$, $\rho_2(t)$, and $\rho_3(t)$, respectively. We set (d) $\lambda = 4\omega_0/\pi$ as the reference in III B-D.

lyzed by diagonalizing the three-state Hamiltonian described by Ω_j and Δ_{jk} . Then the time evolution $\rho_j(t)$ is, for example, characterized by three frequencies $\Omega_R = 1.04\omega_0$, $\epsilon_-/\hbar = 1.02\omega_0$, and $\epsilon_+/\hbar = 0.0196\omega_0$, corresponding to the three transition frequencies between eigenstates (see Appendix B). This feature is peculiar to the multistate system in contrast to the two-state case, where the motion is characterized by the Rabi frequency in NMR.

As λ increases, the energy exchange between the $|j\rangle$ states and the bath becomes efficient and the low frequency part of the coherent motion is suppressed as illustrated Figs. 2(b) and 2(c). The population of $|1\rangle$ undergoes the transition to $|3\rangle$ and eventually decays exponentially as illustrated in Fig. 2(d). If the λ becomes even larger, $\rho_j(t)$ quickly reaches to its equilibrium value as can be seen in Fig. 2(e). If we regard the canonically transformed (P, Q) oscillator plus bath system as the bath for the three-state system, the condi-

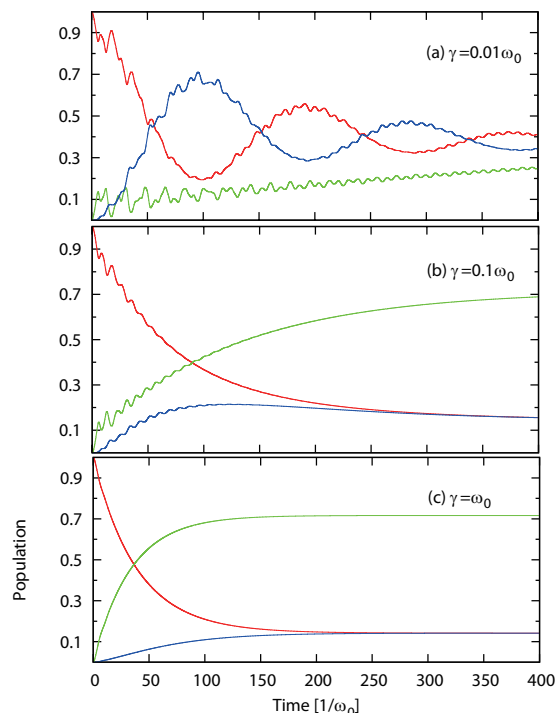


FIG. 3. Time-evolution of the density matrix elements for different oscillator-bath coupling $\gamma =$ (a) $0.01\omega_0$, (b) $0.1\omega_0$, and (c) ω_0 . We set $\lambda = 4\omega_0/\pi$, so that the case (b) $0.1\omega_0$ agrees with Fig. 2(d). The other parameters are the same as Fig. 2. In each figure, the red, green, and blue lines show $\rho_1(t)$, $\rho_2(t)$, and $\rho_3(t)$, respectively.

tions in Figs. 2(d) and 2(e) are in the strong system-bath coupling regime which could not be handled by other reduced equation of motion approaches. If we adopt this picture, the coupling to the transformed bath causes frequency modulations of $|j\rangle$ and thereby shifts the eigenenergies of $|1\rangle$ and $|3\rangle$ states to $\Omega'_1 = \Omega_1 - \lambda/4$ and $\Omega'_3 = \Omega_3 - \lambda/4$, respectively. Thus, while the equilibrium populations ρ_2^{eq} decrease, those of ρ_1^{eq} and ρ_3^{eq} increase for large λ as illustrated in Figs. 2(c)–2(e).

B. Effects of the oscillator-bath coupling strength γ

The parameter γ represents the coupling strength between the (P, Q) mode and the bath. It reflects the time evolution of $\rho_j(t)$ through $J'(\omega)$ defined by Eq. (5). In Fig. 3, we display $\rho_j(t)$ for different γ for fixed $\lambda = 4\omega_0/\pi$. The other parameters are the same as in Fig. 2. Figure 3(a) $\gamma = 0.01\omega_0$ is an underdamped case, whereas Fig. 3(c) $\gamma = \omega_0$ is an overdamped case for the (P, Q) space wavepacket motion.

In this model, the relaxation of the (P, Q) oscillator mode to thermal equilibrium state must be faster than the ET process, otherwise the bath does not play a role. This means that for small γ the ET reaction rate must be much smaller than γ .⁶⁵ We have checked that the choice of γ in the present study satisfies this criteria.

When γ increases, the oscillatory motions in the (P, Q) potentials are suppressed as can be seen from Figs. 3(a)–3(c). Note that the effective coupling strength between the three-level system and the canonically transformed bath is evaluated as $J'(\omega = \Omega)/\Omega$,⁷⁶ where Ω is a characteristic frequency of the three-state system. Thus, $\rho_j(t)$ reaches their equilib-

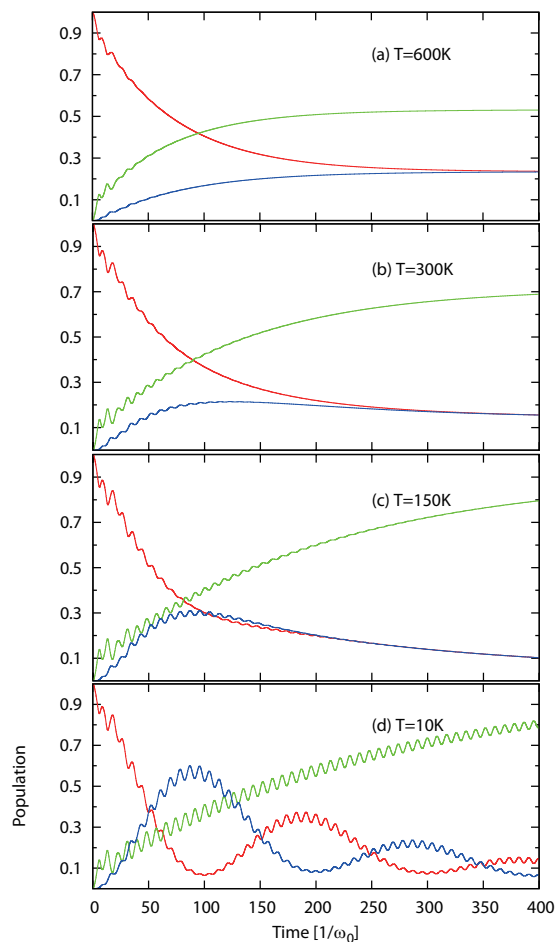


FIG. 4. Time-evolution of the density matrix elements for different temperature T =(a) 600 K, (b) 300 K, (c) 150 K, and (d) 10 K. We set $\lambda=4\omega_0$, so that the other parameters are the same as in Fig. 2. In each figure, the red, green, and blue lines show $\rho_1(t)$, $\rho_2(t)$, and $\rho_3(t)$, respectively.

rium values faster when γ becomes larger because $J'(\omega=\Omega)/\Omega$ becomes larger. The strength of the effective damping for fast components Ω_R and ϵ_-/\hbar is in the order of (b) > (a) > (c), whereas that for slow components ϵ_+/\hbar is (c) > (b) > (a), which results in the fact that the relaxation profiles of $\rho_j(t)$ are different even for the same λ .

C. Effects of the temperature T

Figures 4(a)–4(d) show the time evolution of $\rho_j(t)$ for various temperatures T . In these figures, the displacement is chosen to give $\lambda=4\omega_0/\pi$. The other parameters are the same as those in Fig. 2. When T goes down, the population of the $|2\rangle$ state increases since the energy of this state is the lowest in the present oscillators configuration. At any temperature fast oscillations are the result of (P, Q) motion. When T goes down, the low-frequency oscillation originating from the transition between the electronic states becomes prominent. This is because the excited state motion of the (P, Q) mode, which can smear the electronic transition energies, is suppressed at temperatures below $T=150$ K. While ρ_1 decays exponentially at high temperature, it does not at $T=10$ K, since the dissipative (P, Q) oscillator mode plays a minor role.

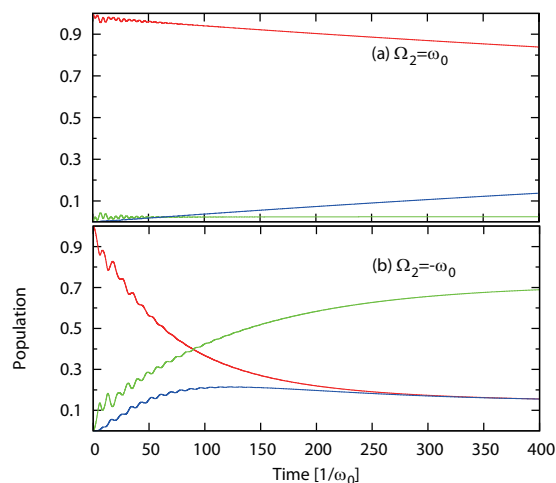


FIG. 5. Time-evolution of the density matrix elements for (a) $\Omega_2=\omega_0$ and (b) $\Omega_2=-\omega_0$. We set $\lambda=4\omega_0/\pi$, $\gamma=0.1\omega_0$ and $T=300$ K so that the case (b) $\Omega_2=-\omega_0$ agrees with Fig. 2(d). In each figure, the red, green, and blue lines show $\rho_1(t)$, $\rho_2(t)$, and $\rho_3(t)$, respectively.

D. Effects of the intermediate state energy Ω_2

We now change the intermediate state energy Ω_2 , which is important to understand a role of activation energy in the ET process. Since we deal with a colored noise, the effective coupling strength $J'(\omega=\Omega)/\Omega$,⁷⁶ where Ω is a characteristic frequency, changes if Ω_j and Δ_{jk} change. To see the pure effects from the configuration, we compare the results with $\Omega_2=\pm\omega_0$ and $\Omega_2=\pm 10\omega_0$, which are illustrated in Figs. 5 and 6. While time-evolution profiles for plus and minus results are similar for large $|\Omega_2|$, they are very different for small $|\Omega_2|$. This is due to the energy shifts of the electronic states arising from the interaction between the system and the canonically transformed bath. The system-bath interaction $-\hat{V}\sum_{\alpha}c'_{\alpha}x'_{\alpha}$ induces energy fluctuations, which shift the energies of $|1\rangle$ and $|3\rangle$ states to $\Omega'_1=\Omega_1-\lambda/4$ and $\Omega'_3=\Omega_3-\lambda/4$. Since the effective damping strength is determined by $|\Omega_2-\Omega'_1|$ and $|\Omega_2-\Omega'_3|$, the difference of damping for positive and negative $|\Omega_2|$ becomes large for small Ω_2 . Thus, while the results in Figs. 5(a) and 5(b) are very different, those in Fig. 6(a) and 6(b) are similar.

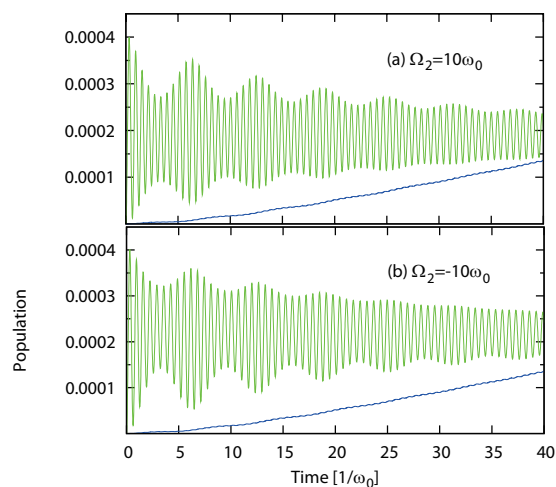


FIG. 6. Same as in Fig. 5 besides (a) $\Omega_2=10\omega_0$ and (b) $\Omega_2=-10\omega_0$.

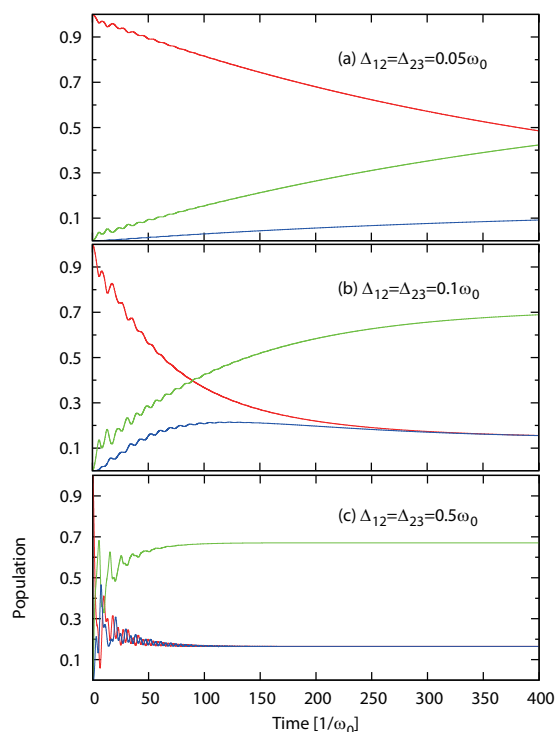


FIG. 7. Time-evolution of the density matrix elements for different nonadiabatic couplings $\Delta_{12}=\Delta_{23}$ =(a) $0.05\omega_0$, (b) $0.1\omega_0$, and (c) $0.5\omega_0$. We set $\lambda=4\omega_0/\pi$, $\gamma=0.1\omega_0$ and $T=300$ K. The case (b) $\Delta_{12}=\Delta_{23}=0.1\omega_0$ agree with Fig. 2(d). In each figure, the red, green, and blue lines show $\rho_1(t)$, $\rho_2(t)$, and $\rho_3(t)$, respectively.

E. Effects of the nonadiabatic coupling Δ_{jk}

Finally we discuss the effects of the nonadiabatic couplings Δ_{12} and Δ_{23} , which control the ET reaction in direct manner. Figures 7(a)–7(c) display the time evolution of $\rho_j(t)$ for different nonadiabatic coupling strengths Δ_{12} and Δ_{23} . For weak nonadiabatic coupling, as shown in Fig. 7(a), the populations decay slowly. This result is in the nonadiabatic regime and the ET can be treated as the perturbation of the nonadiabatic coupling. The lowest order transition from $|1\rangle$ to $|3\rangle$ is second-order in both Δ_{12} and Δ_{23} and proportional to $\Delta_{12}^2\Delta_{23}^2$ (see Appendix B). When the nonadiabatic coupling becomes strong, higher-order contributions corresponding to the recrossing processes play a role. This is the diabatic transition regime where the diabatic representation of the potentials is applied to understand system dynamics (see, for example, Fig. 2 in Ref. 20). The populations exhibit oscillating features in the large nonadiabatic coupling case until about $t=50$. In the classical picture, this phenomenon is explained by recrossing of the wavepacket between the potentials that failed to get trapped by dissipation process, but in the quantum picture, it is an interference phenomenon explained by the transition between the energy eigenstates.²⁰

IV. ET REACTION RATE

As shown in Sec. III, $\rho_j(t)$ decays more or less exponentially apart from the initial temporal oscillatory motions. Since the chemical reaction rate can be defined by the flux-flux correlation function, which is the correlation function between the population of reactant and product states, the

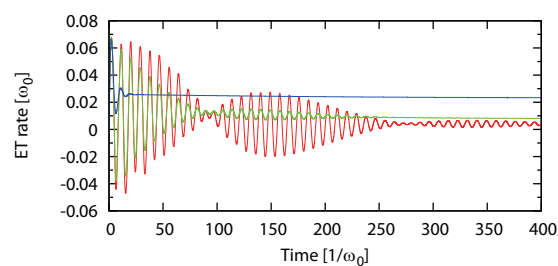


FIG. 8. ET reaction rates $k(t)$ for $\gamma=0.05\omega_0$ (red line), $0.1\omega_0$ (green line), and ω_0 (blue line). The other parameters are the same as in Fig. 3

present ET reaction process may also be characterized by $\rho_j(t)$. Because the difference from the equilibrium population $\delta\rho(t)=\rho(t)-\rho^{eq}$ is expected to approach zero with time as $\delta\rho(t)=\delta\rho(0)\cdot e^{-kt}$, the ET rate can be defined in a time-dependent form⁷⁷

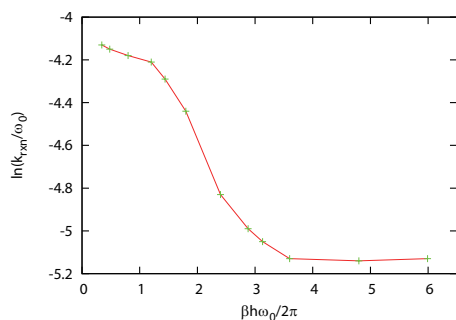
$$k(t) = -\frac{\dot{\delta\rho}(t)}{\delta\rho(t)}. \quad (19)$$

In order to obtain the rate in the three-state ET reaction, we computationally perform linear response experiments.^{68,76} First, we set the energy of the $|3\rangle$ state to $\Omega_3+\epsilon$, where ϵ is small ($0.01\omega_0$) and the populations of electronic states to their thermodynamic averages. After a sufficient time, for which the system reaches equilibrium, we set the present time as $t=0$ and remove the perturbation ϵ . The populations at $t=0$, equilibrated with the perturbation, are no longer in equilibrium and re-equilibrate to the unperturbed state. Then, we adapt the definition of the time-dependent ET rate, Eq. (19), for the three-state system as $k(t) = -\dot{\delta\rho}_3(t)/\delta\rho_3(t)$. Since $\delta\rho_3(t)$ and $\dot{\delta\rho}_3(t)$ are expected to be proportional to the perturbation ϵ if ϵ is small, $k(t)$ does not depend on ϵ .

To illustrate the feature of ET rates, we plot the ET reaction rate as a function of time for different γ in Fig. 8. The other parameters are the same as the case in Fig. 3. For weak γ , ET rates show an oscillation feature, because of the interference of transition between the discrete energy states at different potentials.⁷⁶ In a classical picture, the oscillation feature is interpreted as the recrossing of the population between the potentials caused by the electron that is not trapped.²⁰ After the temporal motions ends owing to the dissipation arising from the bath, the ET rate reaches plateau values. These plateau values, hereafter denoted by k_{rxn} , correspond to the relaxation rates. In the following, we plotted k_{rxn} as the function of T , Ω_2 , and Ω_1 to characterize the ET processes.

A. ET rate as a function of inverse temperature

Figure 9 displays k_{rxn} as the function of the inverse temperature $\beta\hbar\omega_0$. To analyze the temperature dependence of k_{rxn} , it is helpful to adopt the diabatic picture of the ET processes. The activation energies in this picture are estimated from the difference between the potential minima and the crossing points of the potentials. The activation energies between $|1\rangle$ and $|2\rangle$ and $|2\rangle$ and $|3\rangle$ are then evaluated as $E_{12}^\ddagger=0.104\hbar\omega_0$ and $E_{23}^\ddagger=0.785\hbar\omega_0$, respectively. Since we

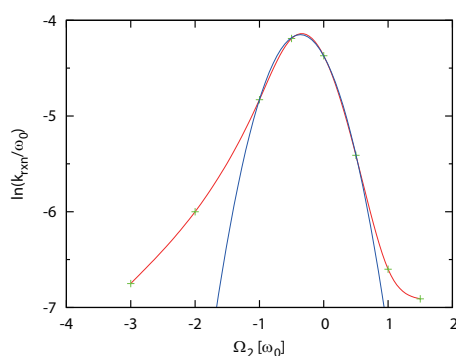
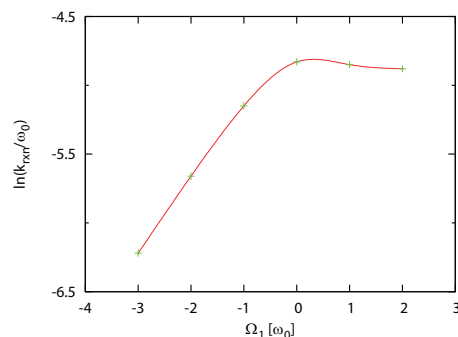
FIG. 9. The relaxation rate k_{rxn} as a function of the inverse temperature.

defined the ET rate by Eq. (19), the reactant state involves both the $|1\rangle$ and $|2\rangle$ states. When the temperature is high ($\beta\hbar\omega_0 < 1$), both $|1\rangle$ and $|2\rangle$ states are populated and both $|1\rangle \rightarrow |2\rangle \rightarrow |3\rangle$ and $|2\rangle \rightarrow |3\rangle$ transitions contribute to the ET rate. Since the $|1\rangle$ to $|3\rangle$ transition is harder than $|2\rangle$ to $|3\rangle$ and population in the $|1\rangle$ state cannot be negligible for $\beta\hbar\omega_0 < 1$, the gradient of the ET rate as a function of $\beta\hbar\omega_0$ becomes gentle in $\beta\hbar\omega_0 < 1$. The ET rates follows the Arrhenius law of the $|2\rangle \rightarrow |3\rangle$ transition with the activation energy $E_{23}^\ddagger = 0.785\hbar\omega_0$.

The ET process is an intrinsically quantum process and the reaction rate reflects not only energy gaps but also the overlap of wave functions. For low temperature $\beta\hbar\omega_0 > 3.60$, the wavepackets are localized at the ground state of $|2\rangle$. Since the profile of a wavepacket does not change much below this temperature, the ET rate, which can also be calculated from the overlap of integrals of $|2\rangle$ and $|3\rangle$ wavepackets, become constants.

B. ET rate as a function of Ω_2 and Ω_1

Figures 10 and 11 illustrate the ET reaction rates as a function of Ω_2 and Ω_1 evaluated from the linear response simulation. The other parameters are the same as those in Fig. 2. In contrast to the results from the two-state system whose ET rate profile is characterized by so called "inverted parabola" (see also Appendix C),^{1,4,50,60,78} the ET rates in the three-state case exhibits an asymmetric bell shape as shown in Fig. 10. The top of the parabola is not formed at $\Omega_2 = 0$ but at $\Omega_2 = -\lambda/4$, since the (P, Q) oscillator plus bath system shifts the energies of both the $|1\rangle$ and $|3\rangle$ states. For Ω_2

FIG. 10. The relaxation rate k_{rxn} as a function of Ω_2 . We set $\Omega_1 = \Omega_3 = 0$. Resultant values of $\ln(k_{rxn}/\omega_0)$ (green points) are fitted to the spline function (red line), and those of $\Omega_2 = -\omega_0, -0.5\omega_0, 0$, and $0.5\omega_0$ are fitted to the parabola (blue line).FIG. 11. The relaxation rate k_{rxn} as a function of Ω_1 . We set $\Omega_2 = -\omega_0$ and $\Omega_3 = 0$.

$\gg \omega_0$, $\ln k_{rxn}$ does not decrease so much, since the quantal superexchange transition mechanism plays a major role in this parameter regime.^{31,32} This process arises from the coherent transition between $|1\rangle$ and $|3\rangle$, which utilizes the coherences between $|1\rangle$ and $|2\rangle$ and $|2\rangle$ and $|3\rangle$, and is similar to the second-order Raman process in the optical problem.^{79,80} Since the $|2\rangle$ state acts as the virtual state, the Ω_2 dependence of the superexchange transition is weaker than that of the thermally activated transition from $|1\rangle \rightarrow |2\rangle \rightarrow |3\rangle$. This transition is called a sequential transition and is analogous to the luminescence in optics. While the transition for $-\omega_0 < \Omega_2 < 0.5\omega_0$ is explained by the sequential transition which exhibits a normal inverted parabolic profile as a function of Ω_2 , $\ln(k_{rxn}/\omega_0)$ becomes larger than expected for $\Omega_2 < -\omega_0$. As explained before, both $|1\rangle$ and $|2\rangle$ states act as the reactant state by the definition $k(t)$ in Eq. (19). For small Ω_2 , the majority of the population is in the $|2\rangle$ state and the major contribution to the ET rate becomes the $|2\rangle \rightarrow |3\rangle$ transition, while the contribution from $|1\rangle \rightarrow |2\rangle \rightarrow |3\rangle$ transition becomes small due to the small $|1\rangle$ population. Since the transition rate of $|2\rangle \rightarrow |3\rangle$ is larger than that of $|1\rangle \rightarrow |2\rangle \rightarrow |3\rangle$, the ET rate becomes larger than expected from the parabolic profile as indicated in Fig. 10.

Figure 11 displays the ET reaction rate as the function of Ω_1 for fixed $\Omega_2 = -\omega_0$ and $\Omega_3 = 0$. For large Ω_1 , the majority of the population is in the $|2\rangle$ state and since only the $|2\rangle \rightarrow |3\rangle$ transition contributes to the ET rate, the reaction rate becomes constant. For small Ω_1 , most population is in the $|1\rangle$ state. In this case the transition between $|2\rangle$ and $|3\rangle$ plays a minor role and the ET rate is mostly determined from the $|1\rangle \rightarrow |2\rangle$ transition. Then the profile of the ET rate exhibits an inverted parabolic shape for small Ω_1 with the activation energy determined from the $|1\rangle$ and $|2\rangle$ states.

V. CONCLUDING REMARKS

In this paper, we study the ET process by employing the hierarchy equations of motion for the Brownian spectral distribution with the low-temperature correction terms.^{19,74} Taking an advantage of nonperturbative theory, we studied ET dynamics and ET reaction rates for the first time over a wide range of parameters including the system-bath coupling, nonadiabatic coupling and temperatures for various oscillators configurations. The time evolution of the reduced density matrix elements illustrates the interplay of coherences

between the electronic and vibrational states. The ET reaction rates as a function of the intermediate state energy exhibits an asymmetric inverted parabolic profile in a small activation regime due to the presence of the intermediate state between the reactant and product states and a slowly decaying profile in a large activation energy regime, which arises from the quantum coherent transitions.

If necessary, further extension to a nonadiabatic transition problem with anharmonic potential surfaces^{20,21} with taking into account nonlinear oscillator-bath coupling^{81,82} is possible from the hierarchy equations of motion approach by explicitly dealing with the oscillator coordinate. Since we are dealing with equations of motion with the system-bath coherence, we can easily include the external time-dependent driving force to the system dynamics. Thus, nonlinear spectroscopy, such as multi-dimensional spectroscopy,⁸³ is easily studied from the hierarchy equations of motion approach. Rigorous numerical solutions from this approach can provide information that can be compared with experimental results and approximate theory.

ACKNOWLEDGMENTS

The authors gratefully acknowledge discussions with Professor Akira Yoshimori (Kyushu University), Dr. Arend G. Dijkstra, and Dr. Hirotaka Nishioka. This work was supported by a Grant-in-Aid for Scientific Research Grant No. B19350011 from the Japan Society for the Promotion of Science.

APPENDIX A: DERIVATION OF HIERARCHY EQUATIONS OF MOTION

The reduced density matrix of this system can be treated by the path-integral formalism by utilizing the coherent state representation. While the conventional coherent state representation is for two-state system,⁶⁶ here we extend it for three-state as $|\psi\rangle = |0\rangle + |1\rangle\phi_1 + |2\rangle\phi_1\phi_2$, where ϕ is a Grassmann number. Since $|\psi\rangle$ is not orthogonal, the completeness relation is then expressed as

$$1 = \int d\bar{\psi}d\psi|\psi\rangle\langle\psi|e^{-\bar{\phi}_1\bar{\phi}_2\phi_1\phi_2-\bar{\phi}_2\phi_2} \\ \equiv \int d\bar{\phi}_1d\bar{\phi}_2d\phi_2d\phi_1|\psi\rangle\langle\psi|e^{-\bar{\phi}_1\bar{\phi}_2\phi_1\phi_2-\bar{\phi}_2\phi_2}, \quad (\text{A1})$$

where $\langle\psi| = \langle 0| + \bar{\phi}_2\langle 1| + \bar{\phi}_2\bar{\phi}_1\langle 2|$. Hereafter ψ represents a set of two Grassmann numbers $\{\phi_1, \phi_2\}$. The following procedure to derive the equation of motion is parallel to that in the high-temperature Drude distribution case.⁶⁶ In order to have the reduced density matrix elements in a compact form, we employ a temporary initial condition of the total system in the factorized form as $\hat{\rho}_A(t_0) \otimes \hat{\rho}_B^{eq}$, where $\hat{\rho}_B^{eq}$ is the equilibrium density matrix of the bath. This assumption can be removed once we derive the equations of motion by setting $\tau_c \ll -1/\Omega_c$ and by integrating up to time the $t=0$, where τ_c is characteristic relaxation time of the system, to have the correlated initial condition at $t=0$.⁶³

The reduced density matrix element at t is represented as $\rho_{j_1, j_2, \dots, j_K}^{(n,m)}(\psi_f, \psi'_f; t)$ and then that at $t+\epsilon$ is obtained in the path integral form by inserting the completeness relation into the reduced density matrix at t by

$$\rho_{j_1, \dots, j_K}^{(n,m)}(\psi_f, \psi'_f; t + \epsilon) = \text{T} \left(\int d\bar{\psi}d\psi d\bar{\psi}'d\psi' e^{-\bar{\phi}_1\bar{\phi}_2\phi_1\phi_2-\bar{\phi}_2\phi_2} \right. \\ \times \langle\psi_f|e^{-i\hbar\hat{H}_A\epsilon}|\psi\rangle\langle\psi|e^{-i\hbar\hat{H}_A(t-t_0)}|\psi_0\rangle \\ \times F_{j_1, j_2, \dots, j_K}^{(n,m)}(t + \epsilon)\langle\psi'_0|e^{i\hbar\hat{H}_A(t-t_0)}|\psi'\rangle \\ \left. \times \langle\psi'|e^{i\hbar\hat{H}_A\epsilon}|\psi'_f\rangle e^{-\bar{\phi}'_1\bar{\phi}'_2\phi'_1\phi'_2-\bar{\phi}'_2\phi'_2} \right). \quad (\text{A2})$$

We expand both sides of Eq. (A2) with respect to ϵ and integrate the right side with respect to Grassmann numbers $\bar{\psi}, \psi, \bar{\psi}'$, and ψ' following the Berezin's rule. Then by taking the limit ϵ to 0, we have

$$\frac{\partial}{\partial t} \rho_{j_1, \dots, j_K}^{(n,m)}(\psi_f, \psi'_f) = \int d\bar{\psi}d\psi d\bar{\psi}'d\psi' \left\{ -\mathcal{L}^{(n,m)} \rho_{j_1, \dots, j_K}^{(n,m)}(\bar{\psi}, \psi'; t) \right. \\ + V^\times(t) \rho_{j_1, \dots, j_K}^{(n+1,m)}(\bar{\psi}, \psi'; t) \\ + n\Theta_-(t) \rho_{j_1, \dots, j_K}^{(n-1,m)}(\bar{\psi}, \psi'; t) \\ + V^\times(t) \rho_{j_1, \dots, j_K}^{(n,m+1)}(\bar{\psi}, \psi'; t) \\ + m\Theta_+(t) \rho_{j_1, \dots, j_K}^{(n,m-1)}(\bar{\psi}, \psi'; t) \\ + \sum_{k=1}^K V^\times(t) \rho_{j_1, \dots, j_{k+1}, \dots, j_K}^{(n,m)}(\bar{\psi}, \psi'; t) \\ \left. + \sum_{k=1}^K j_k \nu_k \Psi_k(t) \rho_{j_1, \dots, j_{k-1}, \dots, j_K}^{(n,m)}(\bar{\psi}, \psi'; t) \right\}, \quad (\text{A3})$$

where

$$\mathcal{L}^{(n,m)} = \frac{i}{\hbar} (H_A(\bar{\psi}_f, \psi) - H_A(\bar{\psi}', \psi'_f)) \\ + \frac{(n+m)\gamma}{2} - i(n-m)\zeta + \sum_{k=1}^K j_k \nu_k - \Xi(t). \quad (\text{A4})$$

The Eq. (A3) is converted to the hierarchy equations of motion in operator form Eq. (15).

To truncate the infinite hierarchy, we formally solve Eq. (15) as

$$\rho_{j_1, \dots, j_K}^{(n,m)} = \int_{t_0}^t d\tau e^{-\hat{\mathcal{L}}^{(n,m)}(t-\tau)} \hat{g}(\tau), \quad (\text{A5})$$

where $-\hat{\mathcal{L}}^{(n,m)}$ is the operator form of Eq. (A4) defined by Eq. (16) and

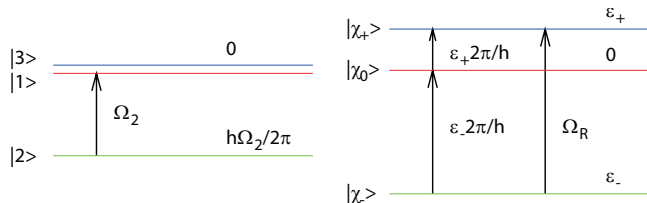


FIG. 12. Schematic view of the nondiagonal energies (left) and eigenenergies (right) of a three-state system. Beside the arrows are the characteristic frequencies of the system Ω_2 (left), ϵ_{\pm}/\hbar , and Ω_R (right).

$$\begin{aligned} \hat{g}(\tau) = & \hat{V}^{\times} \hat{\rho}_{j_1, \dots, j_K}^{(n+1, m)}(\tau) + n \hat{\Theta} \hat{\rho}_{j_1, \dots, j_K}^{(n-1, m)}(\tau) + \hat{V}^{\times} \hat{\rho}_{j_1, \dots, j_K}^{(n, m+1)}(\tau) \\ & + m \hat{\Theta} \hat{\rho}_{j_1, \dots, j_K}^{(n, m-1)}(\tau) + \sum_{k=1}^K \hat{V}^{\times} \hat{\rho}_{j_1, \dots, j_{k-1}, \dots, j_K}^{(n, m)}(\tau) \\ & + \sum_{k=1}^K j_k \nu_k \hat{\Psi}_k \hat{\rho}_{j_1, \dots, j_{k-1}, \dots, j_K}^{(n, m)}(\tau). \end{aligned} \quad (\text{A6})$$

If the condition Eq. (17) is satisfied, $\Gamma^{(n, m)} \equiv (n+m)\gamma/2 + \sum_{k=1}^K j_k \nu_k$ is much larger than the characteristic time of the main system $\{\Omega_l - \Omega_m\}_{lm}$ because $\Gamma^{(n, m)} \geq N_{max} \min(\gamma/2, \nu_1)$. Then Eq. (16) is approximated as

$$\Gamma^{(n, m)} e^{\Gamma^{(n, m)}(t-\tau)} \simeq \delta(t-\tau), \quad (\text{A7})$$

which leads Eq. (15) to Eq. (18).

APPENDIX B: THREE-STATE RABI OSCILLATION

To illustrate the characteristic motion for the three-state system, we analytically solve equation of motion for \hat{H}_A defined by Eq. (2). We consider the probability that the system is initially (at $t=0$) in the state $|1\rangle$ and found in the state $|j\rangle$ at time t defined by

$$P_{j1}(t) \equiv |\langle j|U(t,0)|1\rangle|^2, \quad (\text{B1})$$

where $U(t,0)$ is the time evolution operator. To simplify the results, we assume $\Omega_1 = \Omega_3 = 0$, $\Delta_{12} = \Delta_{21}$, and $\Delta_{23} = \Delta_{32}$. Then the eigenvalues of \hat{H}_A is given by $\epsilon = 0$ and $\epsilon_{\pm} \equiv \hbar(\Omega_2 \pm \Omega_R)/2$, where

$$\Omega_R = \sqrt{\Omega_2^2 + 4(\Delta_{12}^2 + \Delta_{23}^2)} \quad (\text{B2})$$

and the corresponding eigenstates are

$$|\chi_0\rangle = \frac{1}{\sqrt{\Delta_{12}^2 + \Delta_{23}^2}} (\Delta_{23}|1\rangle - \Delta_{12}|3\rangle), \quad (\text{B3})$$

and

$$|\chi_{\pm}\rangle = c_{\pm} \left(\Delta_{12}|1\rangle + \frac{\epsilon_{\pm}}{\hbar}|2\rangle + \Delta_{23}|3\rangle \right), \quad (\text{B4})$$

where $c_{\pm} = (\Delta_{12}^2 + \Delta_{23}^2 + \epsilon_{\pm}^2/\hbar^2)^{-1/2}$ (see Fig. 12).

The time evolution operator is thus expressed as

$$U(t,0) = |\chi_0\rangle\langle\chi_0| + |\chi_+\rangle e^{-i\hbar\epsilon_+t}\langle\chi_+| + |\chi_-\rangle e^{-i\hbar\epsilon_-t}\langle\chi_-|, \quad (\text{B5})$$

in the $|1\rangle$, $|2\rangle$, and $|3\rangle$ basis sets. The probability of the system to be found in the state $|2\rangle$ and $|3\rangle$ at t are given, respectively, by

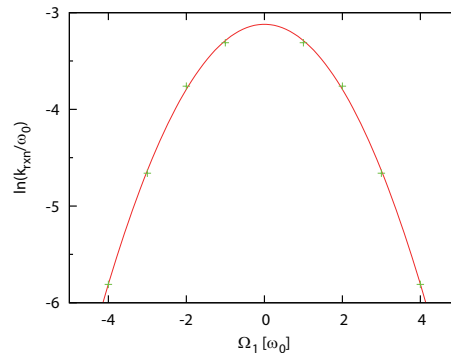


FIG. 13. The ET rate for a two-state system as a function of Ω_1 . Resultant values of $\ln(k_{rxn}/\omega_0)$ (green points) are fitted to the parabola. We set $\Omega_2 = 0$, $\Delta_{12} = \Delta_{21} = 0.1\omega_0$, and $\lambda = 4\omega_0/\pi$. The other bath parameters are the same as in Fig. 3(b).

$$P_{21}(t) = \frac{2\Delta_{12}^2}{\Omega_R^2} \sin^2\left(\frac{\Omega_R}{2}t\right), \quad (\text{B6})$$

and

$$\begin{aligned} P_{31}(t) = & \frac{4\Delta_{12}^2\Delta_{23}^2}{\Delta_{12}^2 + \Delta_{23}^2} \left\{ c_+^2 \sin^2\left(\frac{\epsilon_+}{2\hbar}t\right) + c_-^2 \sin^2\left(\frac{\epsilon_-}{2\hbar}t\right) \right. \\ & \left. - \frac{1}{\Omega_R^2} \sin^2\left(\frac{\Omega_R}{2}t\right) \right\}. \end{aligned} \quad (\text{B7})$$

Thus the oscillation of $\rho_2(t)$ in the Sec. III A depends on Ω_R , while those of $\rho_1(t)$ and $\rho_3(t)$ are determined by Ω_R , ϵ_{\pm}/\hbar , and ϵ_{\pm}/\hbar .

APPENDIX C: ET RATE IN TWO-STATE CASE

We can adapt the hierarchy equations of motion Eqs. (15) and (18) to the two-state case ($|1\rangle$ and $|2\rangle$) by simply truncating the sum of j up to 2 in Eqs. (2) and (4). We set $\Omega_2 = 0$, $\Delta_{12} = \Delta_{21} = 0.1\omega_0$, and $\lambda = 4\omega_0/\pi$ and employ the same bath parameters as in IV B. The ET rate k_{rxn} is defined in terms of $\delta\rho_2(t)$ and the perturbation ϵ is put on Ω_2 to carry out the linear response simulation. Figure 13 shows the ET reaction rate as a function of activation energy at $T=300$. In this low friction regime, the ET reaction rate increases as energy mismatching is small.⁸⁴ The profile for the two-state system is parabolic as predicted by Marcus.

¹R. A. Marcus, *Rev. Mod. Phys.* **65**, 599 (1993).

²V. May and O. Kühn, *Charge and Energy Transfer Dynamics in Molecular Systems* (Wiley-VCH, Berlin, 2003).

³*Electron Transfer from Isolated Molecules to Biomolecules Part 1*, Advances in Chemical Physics Vol 106, edited by J. Jortner and M. Boxin (Wiley, New York, 1999).

⁴S. H. Lin, C. H. Chang, K. K. Liang, R. Chang, Y. J. Shiu, J. M. Zhang, T.-S. Yang, M. Hayashi, and F. C. Hsu, in *Ultrafast Dynamics and Spectroscopy of Bacterial Photosynthetic Reaction Centers*, Advances in Chemical Physics Vol 121, edited by I. Prigogine and S. A. Rice (Wiley, New York, 2002), p. 1.

⁵B. Albinsson and J. Martensson, *J. Photochem. Photobiol., A* **9**, 138 (2008).

⁶L. D. Zusman, *Chem. Phys.* **49**, 295 (1980).

⁷M. Tachiyu, *J. Phys. Chem.* **93**, 7050 (1989).

⁸A. Yoshimori, T. Kakitani, Y. Enomoto, and N. Mataga, *J. Phys. Chem.* **93**, 8316 (1989).

⁹B. Bagchi and G. R. Fleming, *J. Phys. Chem.* **94**, 9 (1990).

¹⁰K. Yoshihara, K. Tominaga, and Y. Nagasawa, *Bull. Chem. Soc. Jpn.* **68**,

- 696 (1995).
- ¹¹ A. Garg, J. N. Onuchic, and V. Ambegaokar, *J. Chem. Phys.* **83**, 4491 (1985).
 - ¹² P. Wolynes, *J. Chem. Phys.* **86**, 1957 (1987).
 - ¹³ S. Mukamel, *Principles of Nuclear Optical Spectroscopy* (Oxford, New York, 1994).
 - ¹⁴ R. Kubo and Y. Toyozawa, *Prog. Theor. Phys.* **12**, 805 (1954).
 - ¹⁵ Y.-J. Yan, M. Sparpaglione, and S. Mukamel, *J. Phys. Chem.* **92**, 4491 (1988).
 - ¹⁶ S. Mukamel and Y. J. Yan, *Acc. Chem. Res.* **22**, 301 (1989).
 - ¹⁷ Y. Hu and S. J. Mukamel, *Chem. Phys.* **91**, 6973 (1989).
 - ¹⁸ G. C. Walker, E. Akesson, A. E. Johnson, N. E. Levinger, and P. F. Barbara, *J. Phys. Chem.* **96**, 3728 (1992).
 - ¹⁹ Y. Tanimura and S. Mukamel, *J. Phys. Soc. Jpn.* **63**, 66 (1994).
 - ²⁰ Y. Tanimura and S. Mukamel, *J. Chem. Phys.* **101**, 3049 (1994).
 - ²¹ Y. Tanimura and Y. Maruyama, *J. Chem. Phys.* **107**, 1779 (1997).
 - ²² D. Egorova, *Chem. Phys.* **347**, 166 (2008).
 - ²³ D. Egorova, M. F. Gelin, M. Thoss, H. Wang, and W. Domcke, *J. Chem. Phys.* **129**, 214303 (2008).
 - ²⁴ M. F. Gelin, D. Egorova, and W. Domcke, *J. Chem. Phys.* **131**, 124505 (2009).
 - ²⁵ R. Kapral and G. Ciccotti, *J. Chem. Phys.* **110**, 8919 (1999).
 - ²⁶ K. Ando and M. Santer, *J. Chem. Phys.* **118**, 10399 (2003).
 - ²⁷ Y. Tanimura and S. Mukamel, *Phys. Rev. E* **47**, 118 (1993); *J. Opt. Soc. Am. B* **10**, 2263 (1993).
 - ²⁸ Y. Tanimura and K. Okumura, *J. Chem. Phys.* **106**, 2078 (1997).
 - ²⁹ M. Bixon, J. Jortner, and M. E. Michael-Beyerle, *Biochim. Biophys. Acta* **1056**, 301 (1991).
 - ³⁰ K. Ando and H. Sumi, *J. Phys. Chem. B* **102**, 10991 (1998).
 - ³¹ T. Kakitani, A. Kimura, and H. Sumi, *J. Phys. Chem.* **103**, 3720 (1999).
 - ³² H. Sumi and T. Kakitani, *J. Phys. Chem. B* **105**, 9603 (2001).
 - ³³ K. Saito, K. Mukai, and H. Sumi, *Chem. Phys.* **326**, 221 (2006).
 - ³⁴ K. Saito and H. Sumi, *J. Chem. Phys.* **131**, 134101 (2009).
 - ³⁵ K. Saito, T. Kikuchi, K. Mukai, and H. Sumi, *Phys. Chem. Chem. Phys.* **11**, 5290 (2009).
 - ³⁶ J. N. Jean, R. A. Friesner, and G. R. Fleming, *J. Chem. Phys.* **96**, 5827 (1992).
 - ³⁷ O. Kühn, V. May, and M. Schreiber, *J. Chem. Phys.* **101**, 10404 (1994).
 - ³⁸ L. Hartmann, J. Goychuk, and P. Hänggi, *J. Chem. Phys.* **113**, 11159 (2000).
 - ³⁹ R. Egger and C. H. Mak, *J. Phys. Chem.* **98**, 9903 (1994).
 - ⁴⁰ M. Topaler and N. Makri, *J. Phys. Chem.* **100**, 4430 (1996).
 - ⁴¹ Y. Jung, R. J. Silbey, and J. Cao, *J. Phys. Chem. A* **103**, 9460 (1999).
 - ⁴² J. Cao and Y. Jung, *J. Chem. Phys.* **112**, 4716 (2000).
 - ⁴³ J. Casado-Pascual, C. Denk, M. Morillo, and R. I. Cukier, *J. Chem. Phys.* **113**, 11176 (2000).
 - ⁴⁴ T. O. Cheche and S. H. Lin, *Chem. Phys.* **274**, 165 (2001).
 - ⁴⁵ B. D. Fainberg and V. A. Gorbunov, *J. Chem. Phys.* **117**, 7222 (2002).
 - ⁴⁶ R. X. Xu, Y. Chen, P. Cui, H. W. Ke, and Y. J. Yan, *J. Phys. Chem. A* **111**, 9618 (2007).
 - ⁴⁷ Q. Shi and E. Geva, *J. Chem. Phys.* **131**, 034511 (2009).
 - ⁴⁸ L. Chen and Q. Shi, *J. Chem. Phys.* **130**, 134505 (2009).
 - ⁴⁹ Q. Shi, L. Chen, G. Nan, R. Xu, and Y. J. Yan, *J. Chem. Phys.* **130**, 164518 (2009).
 - ⁵⁰ K. Ando, *J. Chem. Phys.* **106**, 116 (1997); **114**, 9040 (2001); **114**, 9470 (2001).
 - ⁵¹ K. H. Hughes, C. D. Christ, and I. Burghardt, *J. Chem. Phys.* **131**, 124108 (2009).
 - ⁵² C. Venkataraman, A. V. Soudackov, and S. Hammes-Schiffer, *J. Chem. Phys.* **131**, 154502 (2009).
 - ⁵³ N. Gayathri and B. Bagchi, *J. Phys. Chem.* **100**, 3056 (1996).
 - ⁵⁴ G. L. Closs, L. T. Calcaterra, N. J. Green, K. W. Penfield, and J. R. Miller, *J. Phys. Chem.* **90**, 3673 (1986).
 - ⁵⁵ C. K. Chan, T. J. DiMango, L. X. Q. Chen, and J. R. Fleming, *Proc. Natl. Acad. Sci. U.S.A.* **88**, 11202 (1991).
 - ⁵⁶ Y. Jia, T. J. DiMango, C. K. Chen, Z. Wang, M. Du, D. K. Hanson, M. Schiffer, J. R. Norris, G. R. Fleming, and M. S. Popov, *J. Phys. Chem.* **97**, 13180 (1993).
 - ⁵⁷ G. R. Fleming and R. V. Grondelle, *Phys. Today* **47**(2), 48 (1994).
 - ⁵⁸ T. Arlt, S. Schmidt, W. Kaiser, C. Lauterwasser, M. Mayer, H. Scheer, and W. Zinth, *Proc. Natl. Acad. Sci. U.S.A.* **90**, 11757 (1993).
 - ⁵⁹ B. P. Paulson, H. R. Miller, W. X. Gan, and G. Closs, *J. Am. Chem. Soc.* **127**, 4860 (2005).
 - ⁶⁰ A. Kira, *J. Phys. Chem.* **85**, 3047 (1981).
 - ⁶¹ H. Pal, Y. Nagasawa, K. Tominaga, and K. Yoshihara, *J. Phys. Chem.* **100**, 11964 (1996).
 - ⁶² H. Nakamura, *Nonadiabatic Transition: Concepts, Basic Theories and Applications* (World Scientific, Singapore, 2002).
 - ⁶³ Y. Tanimura, *J. Phys. Soc. Jpn.* **75**, 082001 (2006).
 - ⁶⁴ A. J. Leggett, S. Chakravarty, A. T. Dorsey, M. P. A. Fisher, A. Garg, and W. Zwerger, *Rev. Mod. Phys.* **59**, 1 (1987).
 - ⁶⁵ I. Goychuk and P. Hänggi, in *Quantum Dynamics in Strong Fluctuating Fields*, Advances in Physics Vol. 54 (Taylor and Francis, London, 2005) p. 525.
 - ⁶⁶ Y. Tanimura and R. Kubo, *J. Phys. Soc. Jpn.* **58**, 101 (1989).
 - ⁶⁷ Y. Tanimura, *Phys. Rev. A* **41**, 6676 (1990).
 - ⁶⁸ Y. Tanimura and P. G. Wolynes, *Phys. Rev. A* **43**, 4131 (1991).
 - ⁶⁹ Y. Yan, F. Yang, Y. Liu, and J. Shao, *Chem. Phys. Lett.* **395**, 216 (2004).
 - ⁷⁰ A. Ishizaki and Y. Tanimura, *J. Phys. Soc. Jpn.* **74**, 3131 (2005).
 - ⁷¹ R. X. Xu, P. Cui, Q.-X. Li, Y. Mo, and Y. J. Yan, *J. Chem. Phys.* **122**, 041103 (2005).
 - ⁷² A. Ishizaki and G. R. Fleming, *Proc. Natl. Acad. Sci. U.S.A.* **106**, 17255 (2009).
 - ⁷³ J. Strümpfer and K. Schulten, *J. Chem. Phys.* **131**, 225101 (2009).
 - ⁷⁴ M. Tanaka and Y. Tanimura, *J. Phys. Soc. Jpn.* **78**, 073802 (2009).
 - ⁷⁵ J. Deisenhofer and H. Michel, *Science* **245**, 1463 (1989).
 - ⁷⁶ Y. Tanimura and P. G. Wolynes, *J. Chem. Phys.* **96**, 8485 (1992).
 - ⁷⁷ P. G. Wolynes, in *Lectures in the Science of Complexity, SFI Studies in the Sciences of Complexity*, edited by D. Stein (Addison-Wesley Longman, Reading, MA, 1989), p. 355.
 - ⁷⁸ R. A. Marcus and P. Siders, *J. Phys. Chem.* **86**, 622 (1982).
 - ⁷⁹ T. Takagahara, E. Hanamura, and R. Kubo, *J. Phys. Soc. Jpn.* **43**, 802 (1977).
 - ⁸⁰ Y. Tanimura, T. Suzuki, and R. Kubo, *J. Phys. Soc. Jpn.* **58**, 1850 (1989).
 - ⁸¹ T. Steffen and Y. Tanimura, *J. Phys. Soc. Jpn.* **69**, 3115 (2000).
 - ⁸² T. Kato and Y. Tanimura, *J. Chem. Phys.* **117**, 6221 (2002).
 - ⁸³ Y. Tanimura and A. Ishizaki, *Acc. Chem. Res.* **42**, 1270 (2009).
 - ⁸⁴ J. N. Onuchic and P. G. Wolynes, *J. Phys. Chem.* **92**, 6495 (1988).